A laboratory study of the minimum wind speed for wind wave generation

By KIMMO K. KAHMA† AND MARK A. DONELAN

National Water Research Institute, Canada Centre for Inland Waters, Burlington,
Ontario, Canada, L7R 4A6

The minimum wind speed for wind wave generation has been investigated in a laboratory wind-wave flume using a sensitive slope gauge to measure the initial wavelets about 10 μm high. The growth at very low wind speeds was higher than predicted by the viscous shear-flow instability theory. Assuming that the growth is exponential, the inception wind speed at which the growth rate becomes positive can be defined. It occurred at (friction velocity) $u_* \approx 2$ cm/s, somewhat lower than the $u_* \approx 4$–5 cm/s predicted by shear-flow instability theory. However, the observed growth rates were close to the theory at higher wind speeds when the waves were higher than 1 mm. The effect of temperature on the wind speed at which the waves become readily visible is shown to be appreciable and in keeping with the temperature dependent viscous damping. Other sources of growth are discussed. Our estimates show that the Phillips resonance mechanism might be sufficiently effective to generate the observed growth at very low wind speeds.

1. Introduction

The clarification of the mechanisms for wave generation by wind remains one of the elusive goals of fluid mechanics. Following Ursell's (1956) critical review of the state of knowledge, research activity has increased substantially and a great deal of theoretical and experimental progress has been made. However, consistent experimental verification of theoretical ideas has not been forthcoming, owing, on the one hand, to the mathematical difficulties of dealing with highly turbulent flow over a complex moving boundary leading to unrealistic idealizations, and, on the other hand, to the formidable problems associated with the measurement of direct energy input to waves from wind. The special case of initiation of waves on an initially quiescent liquid surface in response to aerodynamically smooth gas flow lends itself more readily to realistic theoretical formulation since the problem can be restricted to sheared laminar boundary layers. At the same time, the theory produces a result – the minimum wind speed required to produce wave growth – that is, in principle, readily observable. Our purpose here is to test theories for initiation of wave growth by wind in carefully controlled laboratory experiments. Since viscous damping affects the net growth rate, we explore the effect of viscosity (through temperature) on the minimum speed.

Several active microwave remote sensing techniques rely on changes in surface reflectivity caused by short gravity, gravity–capillary and capillary waves. These are the waves that respond to the lightest winds and are most easily suppressed by viscosity. Improvements in our understanding and interpretation of microwave

† Present address: Institute of Marine Research, PO Box 33, SF-00931, Helsinki, Finland

remote sensing of such things as oceanic waves and surface winds depends on clarification of the mechanisms of growth and decay of short wind waves.

A number of theoretical and experimental studies suggest that wind waves are initiated by a viscous shear-flow instability mechanism (e.g. Benjamin 1959; Miles 1962; Valenzuela 1976; Kawai 1979a; van Gastel, Janssen & Komen 1985). Fewer studies have dealt with the minimum wind speed that is required to generate waves, and the results are somewhat controversial. Theoretically, a friction velocity, u_* of about 5 cm/s or a wind speed of about 1.3 m/s (assuming aerodynamically smooth flow) should suffice to generate waves on clean water, but the minimum wind speeds reported from laboratory experiments vary considerably and are usually about twice as high: e.g. Keulegan (1951) 3.3 m/s; Kunishi (1957) 2.4 m/s; Pierson & Stacy (1973) 3.3 m/s; Wu (1978) 1.6 m/s; Pokazeyev & Voronin (1982) 3.2–5.4 m/s. Outdoors somewhat lower speeds are reported: Scott Russell (1844) 0.85 m/s; Jeffreys (1924) 1.1 m/s; Roll (1951) 0.4 m/s; Van Dorn (1953) 2 m/s.

It is important to note that there are, in fact, two different wind speeds to consider: the inception wind speed U_i at which the waves start to grow, and the minimum wind speed that is necessary to generate readily visible or measurable waves. We hereafter refer to this latter as the critical wind speed U_{cr}. The first one should be practically independent of fetch (the properties of the surface drift layer in the water contribute to the theoretical growth rate so that weak fetch dependence may be possible). The latter on the other hand, as pointed out by Kawai (1979b), should be fetch and time dependent. Even when the waves grow, it takes time and fetch before they reach the necessary height to be readily observable.

Most published empirical data are about this latter critical wind speed. The authors often note that its definition is somewhat arbitrary and, e.g. Plate, Chang & Hidy (1969) who were able to measure very small waves, define their critical wind speed not by the smallest observable waves but as a speed at which the appearance of the surface changes from regular to irregular. Their experiment showed that, at short fetches at least, this critical wind speed indeed depends on fetch. In this study, we have used a definition of critical wind speed that is based on the r.m.s. slope of the waves. Judged by the visual appearance of the surface our criterion is close to the criterion of Plate et $al.$ (1969). Somewhat different definitions have been used by Wu (1978), Pokazeyev & Voronin (1982), and Pierson & Stacy (1973).

Previous experimental results regarding the inception wind speed are scarce and comparisons with the coupled shear flow instability theory (Valenzuela 1976; Kawai 1979b) have been done only for friction velocities higher than 10 cm/s. Kawai (1979b) has calculated theoretical growth rates from his model at several wind speeds close to the inception wind speed but these have not been compared with measurements.

2. The experiment

The wind-wave flume was open-ended, being 59 cm wide by 91 cm high and 13.9 m long. It contained water to a depth of 39 cm (figure 1). A variable speed axial-flow fan drew air through the flume. The fan was separated by a canvas joint from the rest of the flume in order to reduce the fan vibrations in the test section. For wind speeds below 1 m/s a separate fan was installed downstream of the main fan. This additional fan was separated by another flexible joint. In the inlet the airflow first passed through a grid, then through a honeycomb which consisted of 1.5 cm diameter tubes after which there was a contraction section with an area ratio of 4:1. The fetch
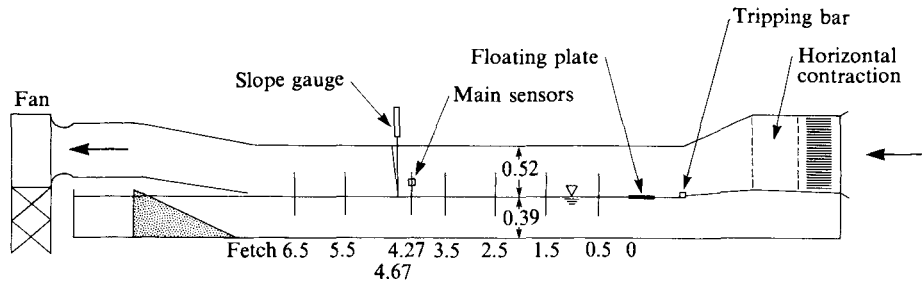
FIGURE 1. The wind-wave flume.

began from the downstream edge of a floating plywood plate 240 cm beyond the horizontal contraction. A 3 cm high tripping bar was placed 110 cm before zero fetch. The top of the plywood plate was only 3 mm above the water surface and the downstream edge was bevelled at 45°.

Water surface displacement, mean air velocity and Reynolds stress in the air were measured at 4.27 m fetch; wave slope was measured at 4.67 m fetch. Other measurements include air temperature, water temperature, and surface tension. The velocity profile in the air and the surface drift current were measured in some instances.

Before describing the details of the instrumentation we will discuss some technical problems associated with measuring wind waves at very low wind speeds. First, the surface film, which always causes some difficulties in laboratory experiments, becomes a much more serious problem when the wind is low. Within one or two days of filling the flume, the contaminants from the air seemed to create a strong surface film with a surface tension as low as 50 mN/m. With appropriate lighting the film is easily discernible. When a moderately high wind (< 9 m/s) was turned on, the surface of the water remained unruffled until the wind stress pushed the film towards the downwind end of the flume. The streamwise length of the horizontally compressed film depends on the wind stress; $u_* > 10$ cm/s or a free-stream velocity $U > 3$m/s was usually sufficient to push such a film beyond the test section in the middle of our flume. This behaviour of the surface film might explain why some authors report that there is a distinct critical wind speed at which the waves start to grow, and why this wind speed can be quite large and is different in different experiments.

To clean the surface we used the standard method of allowing the water to overflow in the downwind end and using the wind to push the film there. A small portion of the film remained, however, in the downwind end of the flume and it slowly spread over the whole surface after the wind was turned off. The remaining film was so weak that we could not detect it by measuring the surface tension, but when the wind was on, its boundary could be seen by tracing those specks of dust that travelled with the surface drift. The specks abruptly stop at the film. In addition, a very weak optical interface could be seen in suitable light. This residual film had to be removed before measurements at low wind speed could be made. To clear the surface completely we first pushed the film away with a slightly higher wind, then lowered the wind, let the seiche decay for a few minutes, and finally measured the waves just before the film again reached the sensors in the test section. Root-mean-square slope estimates at successive stages during the runs indicated that steady state had been achieved. The seiche was of course not completely damped out, and, although it had an amplitude

of only 10 μm–100 μm, it caused substantial window leakage in the spectral analysis unless it was filtered out before taking Fourier transforms.

There were two other sources of background noise in addition to window leakage from the seiche. First, the fan generated some vibration that caused disturbances on the water surface. For example, Plate *et al.* (1969) found that their fan generated an 18 Hz peak in the spectrum. In our experiment the fan vibrations were not normally noticeable, but when a bucket was filled with water, covered with a glass plate and placed on the bottom of the empty flume, the slope gauge detected the fan vibrations which otherwise were masked by the wind waves.

At wind speeds below 1 m/s when a separate quieter fan was used, the fan vibrations were undetectable. When the wind speed was less than 2 m/s, the fan disturbances were smaller than another important source of noise: the microseisms. These vibrations of the ground are caused mainly by wind-generated waves on oceans (Longuet-Higgins 1950), traffic, industry and smaller local sources like compressors. They vary with time and place but their order of magnitude is usually 1 μm. Spectra of microseisms often have a maximum between 0.1 and 1 Hz, and the spectrum falls very rapidly with increasing frequency. The surface film, which after a couple of days covered the water in the flume, was sufficiently strong to damp out these oscillations, and the surface stayed smooth within the accuracy of our slope gauge. However, when the water was clean the surface was never smooth. The spectra measured at night (see figure 4, $U = 0$) show a similar general fall with frequency as the normal microseisms spectra (e.g. Brune & Oliver 1959). During the daytime, heavy traffic on a nearby highway substantially increased the background. Therefore all measurements at very low wind speeds had to be made at around midnight.

It would have been interesting to compare the local ground motion spectrum and the background wave spectrum. Unfortunately, the nearest seismograph was in Ottawa, about 450 km from our laboratory in Burlington. The local sources might contribute considerably to the frequency range of interest to us and therefore the digitization of the seismograms from Ottawa was not considered worthwhile.

2.1. *Air flow measurements*

The tunnel centreline wind speed, U, was measured by means of a Pitot-static tube at a fetch of 4.27 m and height of 15.6 cm above the water surface. Two centimetres closer to the wall and at a height of 13.1 cm a crossed-film (x-film) anemometer was installed to measure the Reynolds stress. The wind speed and angle of attack sensitivity was established in a calibration tunnel over the wind speed range of 0.5 to 11 m/s both before and after the stress measurements. An iterative procedure was used to determine u' and w', the fluctuating components of horizontal and vertical velocity, from the recorded crossed-film signals. Generally, the anemometer signals were sampled at 200 Hz and this permitted an excellent estimate of the local Reynolds stress $-\overline{u'w'}$. In some cases lower sampling rates were used (100 Hz and 40 Hz) and the truncated Reynolds stress co-spectrum was restored by comparison with non-dimensional plots of co-spectra obtained under similar conditions but sampled at 200 Hz. The friction velocity, u_*, was then estimated using the stress distribution for fully developed channel flow (e.g. Tennekes & Lumley 1972):

$$-\overline{u'w'} + \nu_a \frac{dU}{dz} = u_*^2 \left(1 - \frac{z}{a}\right), \tag{1}$$

where ν_a is the kinematic viscosity of air, $2a$ is the depth of the air layer in the flume and z is the vertical coordinate positive upwards from the water surface. The stress distribution (1) implies that the stress on the ceiling and the water surface have the same magnitude. This is probably a reasonable approximation since the ceiling and walls are of slightly rough moulded fibreglass with undulations having centimetric scales and heights of the order of a few millimetres – quite comparable with the water surface roughness in the wind speed range around the critical wind speed.

The viscous term is negligible at the height of the x-film anemometer and so we have $u_* = 1.42\,(-\overline{u'w'})^{\frac{1}{2}}$. The accuracy of our estimates of friction velocity depend on the turbulence being fully developed – a condition which is encouraged by the tripping bar (at 1.1 m before zero fetch) but not necessarily guaranteed at the 4.27 m fetch (about ten times the depth of the air stream from the tripping bar). In this paper we are largely concerned with very low winds for which the flow is aerodynamically smooth – the thickness of the viscous sublayer, $\delta = 11.5\,\nu_a/u_*$ (Schlichting 1968), exceeds the characteristic height of the waves for wind speeds below 4 m/s. Thus, at these speeds we may use the well-established condition for smooth flow $(u_*z_0/\nu_a = 0.14$, where z_0 is the roughness length or virtual origin of the logarithmic velocity profile). In determining z_0, allowance was made for deviations from a logarithmic profile at the height of wind speed measurement. u_* values were calculated in two ways: (i) using the wake function given in Tennekes & Lumley (1972); (ii) using the logarithmic law. These differed by no more than 13 %, and in all cases the higher value was used. This check yielded friction velocities, from the measured winds at 15.6 cm, that were in agreement (average ratio $= 1.17 \pm 0.2$) with the extrapolated measured values from (1); except for two cases near 2.3 m/s that were anomalously low. In each case we used the higher of the two (calculated and measured) values in figure 6. Note that use of the higher u_* values – giving closest agreement to the instability theory – strengthened our conclusion (§3.1) that the shear-flow instability theory underestimates the growth rates at low wind speeds.

2.2. *Slope measurements*

To be able to measure very small slopes accurately we used a laser beam which was reflected from the water surface and was then detected directly by a 10 mm × 10 mm analog (x,y)-position sensor placed in the ceiling of the flume. The maximum slope that this slope gauge could measure was 5 mrad, which is sufficient for the initial waves. For waves with slightly larger slopes we used a converging lens which increased the range to ± 15 mrad. This ensured substantial overlap in the useful ranges of (laser) slope and (capacitance) displacement gauges. Finally we used a visual method to estimate the r.m.s. slope when it was too large to be measured by the sensor. In this method, the maximum absolute value of the negative slope during 5 s was determined by observing the reflected laser beam on a scale attached to the roof of the flume; then ten such observations were averaged. The calibration in figure 2 indicates that the accuracy was better than ± 20 %, which is acceptable since the slope increased an order of magnitude when the wind speed increased by only 50 %. The visual method had a significant advantage in speed over the slope gauge method and thus permitted a more detailed investigation of the affects of viscosity on the critical wind speed than would otherwise have been possible.

The normal right-hand coordinate system was used with x-axis increasing with fetch and z vertical and positive upwards. In this notation the slope $\partial\eta/\partial x$ on the forward face of the wave is negative.
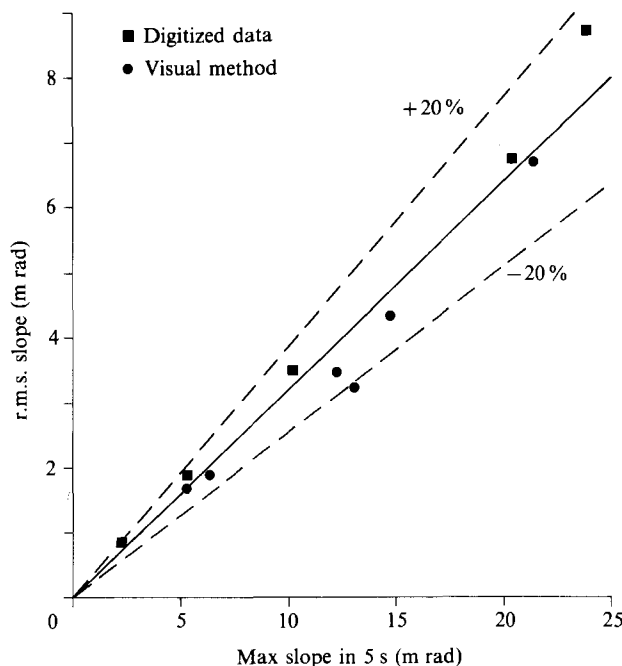
FIGURE 2. Calibration of the visual method to determine the r.m.s. slope.

The slope spectra were transformed into frequency spectra of surface displacement $S(\sigma)$ by

$$S(\sigma) = \frac{\phi_{11}(\sigma) + \phi_{22}(\sigma)}{k^2},\qquad(2)$$

$$c^2 = \frac{\sigma^2}{k^2} = \frac{Tk}{\rho} + \frac{g}{k}\tanh kh,\qquad(3)$$

where $\phi_{11}(\sigma)$, $\phi_{22}(\sigma)$ are x- and y-slope spectra, k is the wave number, T is the surface tension, ρ is the density of water, h is the water depth and g is the acceleration due to gravity (total variance of surface displacement

$$\overline{\eta^2} = \int_0^\infty S(\sigma)\,\mathrm{d}\sigma).$$

The wind generates a surface current v and therefore the apparent frequency is $\omega = k \cdot (c + v)$. However the surface current was not always measured and so we used $v = 0$ when calculating k for equations (2) and (4). The slope spectra were measured only at wind speeds below 3 m/s when the current and the corresponding error is small. Because the elevation spectra from the capacitance gauge are used together with the transformed slope spectra (e.g. in figure 4), and it is not possible to approximate the intrinsic frequency σ by the apparent frequency ω at higher wind speeds without substantial error, we have interpreted the transformed slope spectra as functions of apparent frequency. In this case the true spectrum $S(\omega)$ (as a function of apparent frequency) is slightly larger than the transformed (from slope) spectrum except when $v = 0$. As a function of intrinsic frequency this is also the case unless $S(\sigma)$ decreases with frequency faster than σ^{-5}. Therefore the growth rates are slightly underestimated. This strengthens our case (§3.1) that the theory underpredicts the
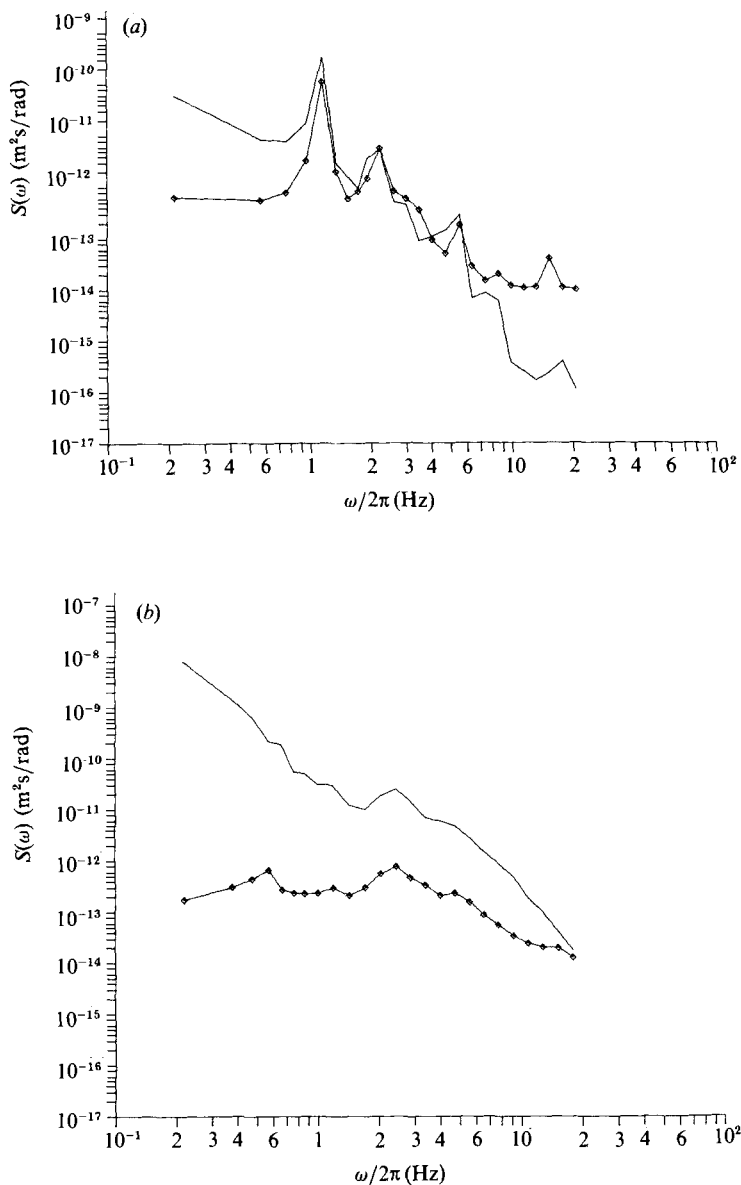
FIGURE 3. Comparison between the displacement spectrum from a capacitance gauge (–◇–) and
the transformed slope spectrum (——). (a) example of agreement found in 50% of the cases;
(b) the worst case observed.

measured growth rate. Doppler shifting due to the orbital motion of the longer waves
(Ataktürk & Katsaros 1987) does not present a problem here since we will need to
transform between slope and displacement or to compute growth rates only for winds
below 4 m/s when the r.m.s. slopes are less than 10^{-2} radians (figure 7) and there is
no appreciable energy in waves with phase speeds in excess of twice the minimum
(figure 4).

When there was no wind the y-slope spectrum $\phi_{22}(\omega)$ was about ten times larger
than the x-slope spectrum $\phi_{11}(\omega)$. To illustrate more clearly the growth of the x-

direction waves, which eventually became dominant, we calculated the following displacement spectrum from the x-slope spectrum

$$S_x(\sigma) = \frac{\phi_{11}(\sigma)}{k^2} = \int_{-\pi}^{\pi} F(\sigma, \theta) \cos^2\theta \, d\theta, \tag{4}$$

where $F(\sigma, \theta)$ is the directional displacement spectrum, the angle θ is measured from the x-axis.

2.3. Surface-displacement measurements

The water surface displacement was measured by a capacitance gauge which consisted of 0.5 mm diameter dielectric-coated transformer wire. This device was sensitive enough to detect waves that were only a few micrometres high, but effects from capillary adhesion make the gauge unreliable at such small wave heights. The shape of the meniscus around the wire depends on the wetting history of the wire, the amount of dirt accumulated on the wire and the properties of the surface film on the water. When the wire is thick and the water surface is dirty, these effects can be significant even when the wave height is as large as one centimetre. Similar results have been reported by, for example, Stalder (1957), Hughes & Grant (1974). Stalder was able to improve the response of his wave gauge to 0.25 mm by wrapping thin strips of tissue paper around the wire. We modified this method and wrapped a very thin cotton thread around the wire (five turns for the full length of the wire), and were able to improve substantially the accuracy and reliability of the gauge. In half of the cases the spectrum agreed well with the displacement spectrum transformed from the slope gauge in the frequency range from 1.5 to 6 Hz. In some cases the waves were only 10 μm high as in the example shown in figure 3(a). In the other half of the cases the agreement was less satisfactory, and it is obviously unacceptable in the worst case shown in figure 3(b). It is interesting to note that the general shape of the spectrum looks roughly correct even in the strongly-damped case. This would suggest that data from a single surface intersecting gauge should be used with caution when measuring such small waves. Since the results from the slope gauge were repeatable with good accuracy we believe that the displacement gauge was indeed contaminated when they compared poorly. In practice it is impossible to predict when the capacitance gauge will give poor results as a tiny surface film slick, originating from dirt in the air may at any time attach to the wire. Therefore, for wave heights less than 1 mm the spectra from the capacitance gauge were used only in conjunction with spectra from the slope gauge.

Figure 4, which is a composite of displacement spectra and transformed spectra, is constructed in the following way: The spectra at 4.0, 6.8, 8.2 and 10 m/s wind speed are from the capacitance gauge. At those wind speeds the wave energy in the y-direction (cross tank) is comparatively negligible. At low wind speeds, when the y-component becomes dominant, the $S_x(\omega)$ spectrum is used for frequencies $\omega > 9.5$ rad/s (1.5 Hz). Because $\phi_{11}(\omega)$ falls below the noise limit when $\omega < 9.5$ rad/s, the transformed spectrum $S_x(\omega)$ would (incorrectly) behave as ω^{-4} at these frequencies, so it is replaced there by the spectrum $S(\omega)$ from the capacitance gauge. (Since $S(\omega)$ is omnidirectional it also shows the cross tank oscillations, in particular, the 6.9 rad/s (1.1 Hz) seiche is very pronounced.) In all spectra shown in this figure, $S(\omega)$ transformed from the slope spectrum and the spectrum from the capacitance gauge agree. There was a difference of 9% (40 cm) in the fetch between these two sensors, but the growth and decay in this short distance were undetectable from the spectra.
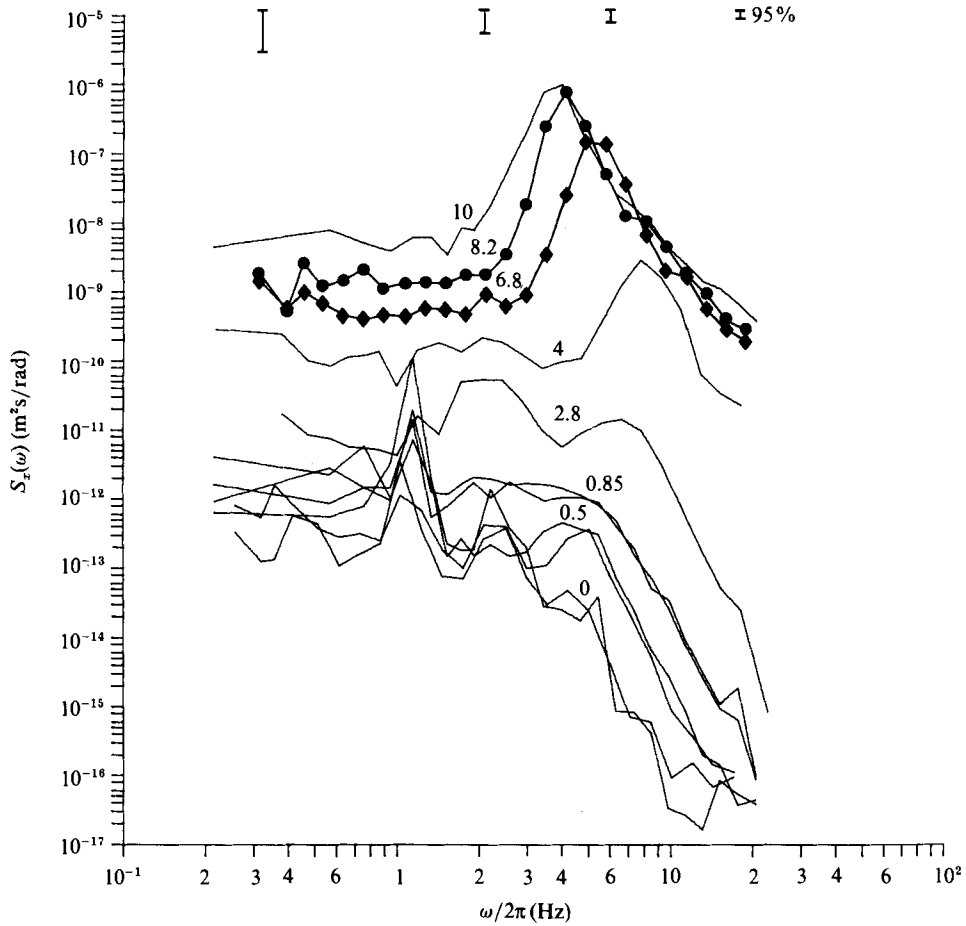
FIGURE 4. The evolution of the frequency spectrum with wind speed (indicated on the figure). The spectra at 0, 0.5, 0.85 and 2.8 m/s wind speed are composites derived from surface displacement spectra and transformed slope spectra.

3. Results

The evolution of the displacement spectrum with wind speed at 25 °C temperature is shown in figure 4. Already at $U = 0.5$ m/s ($u_* = 2.8$ cm/s) the spectrum has risen an order of magnitude above the background level. The characteristic wave height of these waves (when the seiche has been removed) is 10 μm and the peak frequency is 30 rad/s (5 Hz). As the wind increases, the peak moves to higher frequencies up to 55 rad/s (8.7 Hz) when $U = 4$ m/s. Most of this change is due to Doppler shift caused by wind drift. At this speed and below, no part of the spectrum at the 4.27 m fetch is saturated; at that stage it has increased to 10^7 times the background.

3.1. *The inception wind speed*

Because the vibrations of the flume continuously feed energy into the waves, the determination of the inception wind speed is not straightforward. When the wave spectrum at a certain frequency rises above the background it does not necessarily
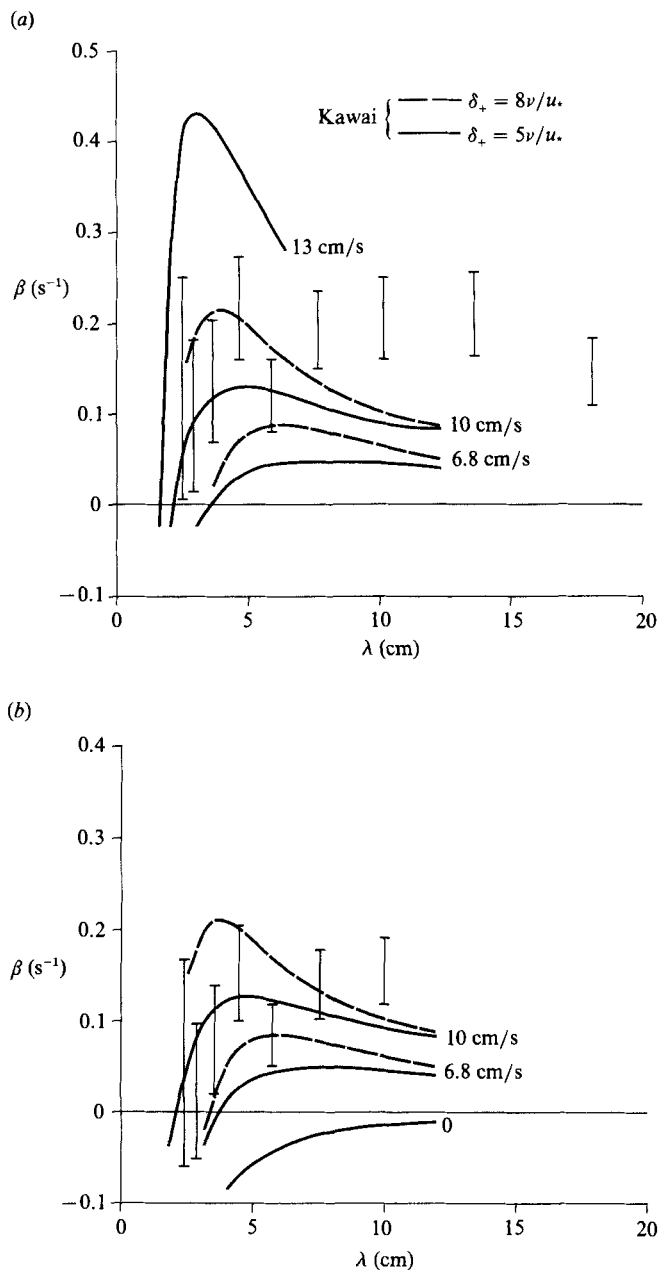
(a)

(b)

FIGURE 5 (a, b). For caption see facing page.

mean that the waves grow as they propagate along the flume. If, for example, the main source of background wave energy were the upwind floating plate, the waves observed at the measuring station would have propagated several metres and lost some energy to viscous dissipation. In sub-inception wind speeds the wind input will reduce the decay rate but not eliminate it; so that even though the waves are larger at the measuring station than they were in the absence of wind, they are still smaller than at their source – the upwind floating plate. To establish the inception wind
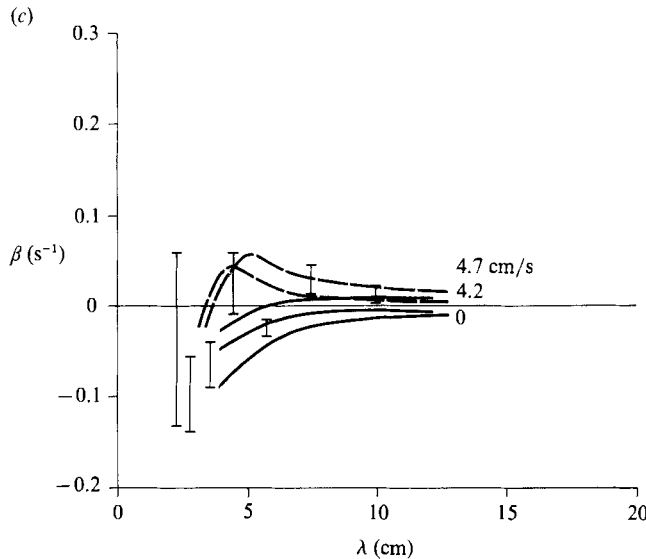
FIGURE 5. Exponential growth rate β for waves in the x-direction ($T_w = 25\ °C$). The bar length refers to the maximum variability which is consistent with (6). The most probable value for β is expected to be close to the minimum of the bar. The curves are from the instability theory (Kawai 1979b). (a) $u_* = 3.4$ cm/s, $U = 0.7$ m/s; (b) $u_* = 2.8$ cm/s, $U = 0.48$ m/s; (c) $u_* = 1.9$ cm/s, $U = 0.35$ m/s.

speed we must determine when the waves could grow even in the absence of the input from vibrations.

We will first analyse the problem from the point of view of the viscous shear-flow instability mechanism. This means that we assume that in the absence of input from vibrations the growth is exponential. In addition, because we observed larger growth than the theory predicts, we will in case of uncertainty choose values of variables that will reduce the difference from the theory. The exponential growth rates presented in figures 5 and 6 are valid only if the dominant growth mechanism is indeed exponential. In §4.2 we will discuss the possibility of direct forcing by turbulent pressure fluctuations (Phillips 1957).

When there is no wind, the dominant direction of waves at the slope gauge is across the flume. The sides of the flume are ineffective in generating waves that propagate in the x-direction, and since the slopes are less than 10 mrad, we do not expect that nonlinearities would change the direction of the waves. The waves that originate in the beach at the downwind end are strongly dissipated by the residual surface film which remains there. Therefore, in the absence of wind the main source of waves propagating in the x-direction should be the plate–water interface at the upwind end. The input to x-direction waves from the sides and the bottom can be assumed to be independent of both the wind speed and the existing wave spectrum. Since this input is small (possibly negligible) we approximate it as a constant term in the energy balance equation for steady waves propagating in the x-direction:

$$(v + c_g(\sigma)) \frac{\partial S_x(\sigma)}{\partial x} = \beta S_x(\sigma) + I(\sigma). \qquad (5)$$

Here $S_x(\sigma)$ is the frequency spectrum (of the x-direction waves), c_g is the group velocity in the absence of a current, $I(\sigma)$ is the input to the x-direction waves from
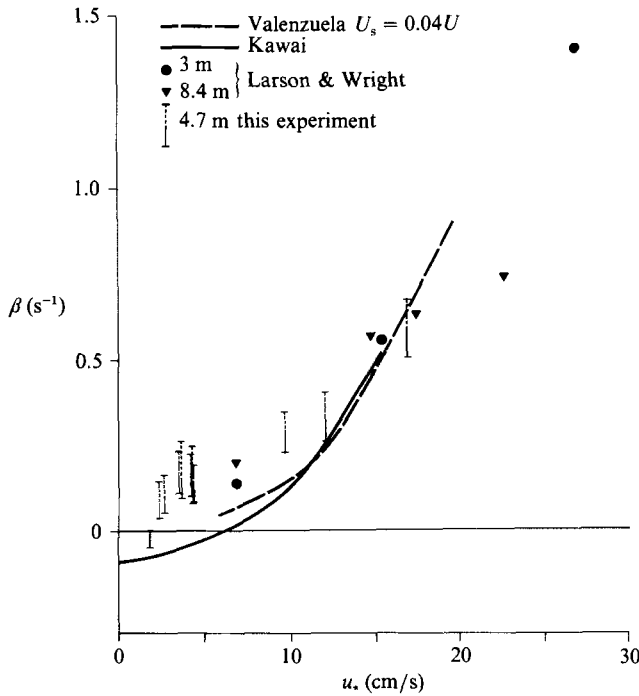
FIGURE 6. Exponential growth rate β for waves in the x-direction ($T_\mathrm{w} = 25\ ^\circ\mathrm{C}$). For our observations the most probable value for β is close to the minimum of the bar.

the bottom and the walls and β is the exponential growth rate. Consistently with our previous choice we will use $v = 0$. (Where the actual downwind current is greater than zero, we will underestimate the growth.) The solution of (5) is then

$$S_x = \left(S_{xp} + \frac{I}{\beta}\right) \mathrm{e}^{\beta x/c_\mathrm{g}} - \frac{I}{\beta} \quad (\beta \neq 0),$$
$$S_x = S_{xp} + Ix/c_\mathrm{g} \qquad\qquad (\beta = 0),$$

(6)

where $S_{xp}(\sigma)$ is the spectrum at the edge of the upwind floating plate (figure 1).

The growth rate β is usually estimated by measuring the waves at two fetches. We could not do this because only one slope gauge and one sensitive wave gauge were available. Six teflon-coated 1.1 mm diameter capacitance wave gauges were installed at fetches 0.5 m, 1.5 m, 2.5 m, 3.5 m, 5.5 m and 6.5 m, but film-dependent meniscus effects on these gauges rendered them too inaccurate for the small waves that occur at wind speeds below 5 m/s. Fortunately, it is possible to estimate the growth rate from measurements at one fetch.

When the wind U is zero, (6) becomes

$$S_{x0} = \left(S_{xp} + \frac{I}{\beta_\mathrm{d}}\right) \mathrm{e}^{\beta_\mathrm{d} x/c_\mathrm{g}} - \frac{I}{\beta_\mathrm{d}},$$

(7)

where $S_{x0}(\sigma)$ is the background spectrum in the absence of wind, and β_d is the exponential decay rate.

When the spectrum is much higher than the background spectrum, the term I can safely be ignored as has been done in previous experiments where growth rates have

been determined. In our case, although we believe that I must be fairly unimportant, we cannot be sure that it is negligible. However, it can be shown that for relevant values of S_x, x and c_g, β is defined implicitly by (6) as a monotonically increasing function of I when $\beta > \beta_d$. In principle, I could be positive or negative (absorbent flume walls), but the sides and the bottom of the flume are hard and so rigidly connected to the great mass of the flume's supporting steel structure that in practice $I > 0$. The minimum of β is therefore obtained when $I = 0$, and in this case we also get an explicit equation for β:

$$\beta = \frac{c_g}{x} \ln \frac{S_x}{S_{x_0}} + \beta_d. \tag{8}$$

Physically this minimum β corresponds to the background being caused by the plate only; we believe that this is close to the actual situation. To ensure that we do not over-estimate β we have used $v = 0$; i.e. we approximate the intrinsic frequency σ by the apparent frequency ω. Since we actually measured the slope spectrum, there are four factors which contribute to the error we make by this approximation. One of them, the Doppler shift in frequency either increases or decreases β depending on the slopes of S_x and S_{x_0} as functions of σ. The three others, the Jacobian $\partial\omega/\partial\sigma$, the shift in k of (4) and the reduction of the growth time $(c_g + v)/x$ in (8) all have the effect of decreasing the estimate below the true temporal growth rate β. For all our measured pairs, S_x, S_{x_0}, the combined effect of the assumption $v = 0$ is to underestimate β.

For waves propagating in the positive x-direction $S_{xp} > 0$. It then follows from (6) that there exists a maximum I, and hence a maximum β, which are obtained when $S_{xp} = 0$. This maximum is of course unrealistic: the bottom and the walls cannot be very effective in generating waves in the x-direction when the end plate is not.

In spite of this we have used the maximum β as an indicator of the confidence limits for our estimates. It is useful to note that these limits are only slightly wider than the scatter of the data of Larson & Wright (1975) or the difference in theoretical growth rates given by Kawai (1979b) caused by the uncertainty of the height of the viscous sublayer.

In a flume, the decay rate can be divided into two terms: $\beta_d = \beta_s + \beta_b$, where β_s is the surface damping coefficient and β_b is the damping coefficient that is related to the dissipation at the bottom and walls of the flume. In order to obtain general results, the contribution from β_b must be eliminated. If β were determined by the usual method using different fetches it would be important to determine β_b accurately. In our case it is sufficient to know that β_b is not the dominant term of β_d. When $I = 0$, β_b will be eliminated completely when (8) is derived from (6) and (7) and it has only a minor influence as long as $\beta_b < \beta_s$.

The theoretical equation for β_s is (Lamb 1932)

$$\beta_s = -4\nu_w k^2. \tag{9}$$

For gravity waves, the theoretical equation for the spatial decay rate which corresponds to β_b can be written (Hunt 1952) for the case of $v = 0$;

$$\frac{1}{S}\frac{\partial S}{\partial x} = -\frac{4k}{b}\frac{kb + \sinh 2kh}{\sinh 2kh + 2kh}\left(\frac{\nu_w}{2\sigma}\right)^{\frac{1}{2}}, \tag{10}$$

where h is the water depth, ν_w is the viscosity of water and b is the width of the flume.

The above equations indicate that in our flume the bottom and wall dissipation

becomes dominant when $\omega < 25$ rad/s (4 Hz) and is about 20 % of β_s at $\omega = 43$ rad/s (6.8 Hz).

The observed spectrum contains noise also. For a given I, additional noise terms in (6) and (7) will increase the β that these equations implicitly define. Because we have ignored the noise, our estimates are on average too small. At $\omega = 40$ rad/s, where the slope spectrum has its maximum, this error can be ignored but above 60 rad/s (9.5 Hz) it becomes significant. When $U = 0$ the spectra (cf. figure 4) show a clear tendency to level off above 60 rad/s, apparently due to the background noise.

The growth rates at the three lowest wind speeds at 25 °C temperature are shown in figure 5. The growth rate is clearly positive when $U = 0.5$ m/s, and if the growth is exponential the inception wind speed is probably about $U = 0.4$ m/s, corresponding to $u_* = 2$ cm/s. The curves show the growth rates predicted by the shear-flow instability calculations of Kawai (1979b). The inception friction velocity from Kawai is 3.8–4.5 cm/s, and at least $u_* = 7$ cm/s is required to obtain the growth rates which we found at $u_* = 3.4$ cm/s.

The 8 cm wavelength of the waves at $u_* = 5$ cm/s is fairly close to that predicted by Kawai but differs substantially from the 2 cm wavelength predicted by van Gastel *et al.* (1985).

The growth rates of Valenzuela (1976) are slightly larger at low wind speeds than those given by Kawai but $u_* = 7$ cm/s is required also according to his results to predict our growth rates at $u_* = 3.4$ cm/s.

Figure 6 shows the growth rate of an $\omega = 43$ rad/s wave component as a function of u_*. This wave component is close to the peak of the spectrum until it saturates. Up to $u_* = 10$ cm/s the measured growth rates are considerably higher than the instability theory predicts. The growth rates from Larson & Wright (1975) agree well with our measurements. Larson & Wright measured the temporal growth of wind generated waves. The maximum fetch was 8.4 m, therefore their wave heights are of the same size as ours.

We want to emphasize that the results above are based on the assumption of exponential growth and that in cases of uncertainty we have in all instances chosen the method or values of parameters which will reduce our estimates of β. The deviation from the theory is therefore probably slightly larger than our results indicate.

Mechanical waves show smaller growth rates that agree better with the theory (Gottifredi & Jameson 1970; Wilson *et al.* 1973). It is, however, not clear how well such experiments, in which a finite monochromatic wave grows, reveal the wind speed appropriate to the inception of wind waves whose r.m.s. slopes are less than 10^{-3} radians (figure 7). We will discuss this further in §4.2.

3.2. *Growth with wind speed*

Figure 7 shows how the characteristic wave height H_c (4 × r.m.s. surface displacement), r.m.s. x-slope and the spectrum $S_x(\omega)$ at $\omega = 43$ rad/s (6.8 Hz) grow with wind speed. The close agreement between these three (after a suitable scaling factor has been used) is a consequence of the fact that the frequency of the peak of the spectrum moves only from 30 rad/s (5 Hz) to 55 rad/s (8.7 Hz) before the rear face of the spectrum (frequencies above the peak frequency) becomes saturated at a wind speed of about 5 m/s. When the wind speed increases, the characteristic wave height increases first relatively slowly from the 10 µm background level to 50 µm at
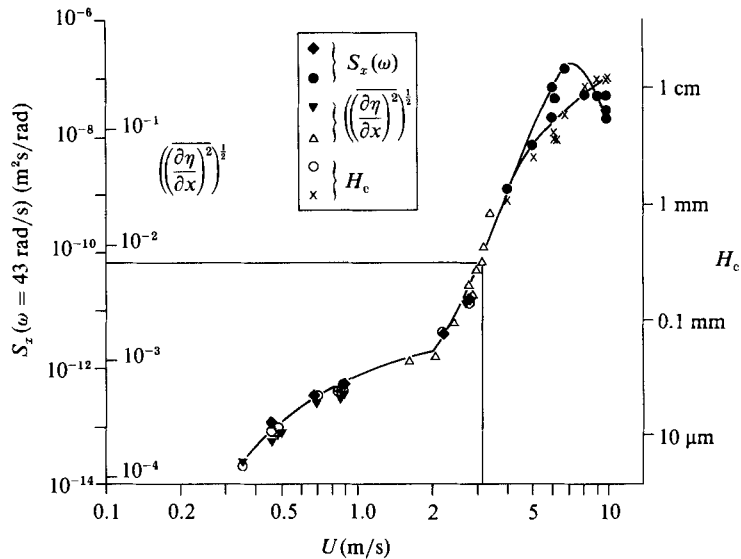
FIGURE 7. Growth *vs.* wind speed of a single component of the displacement spectrum near the peak (◆, ●); r.m.s. slope (▼, △); and characteristic wave height (○, ×). The measurement methods used were: ◆, ▼, ○, slope gauge; ●, ×, capacitance gauge; △, visual method. The vertical line shows the critical wind speed which corresponds to 6.6 mrad r.m.s. slope. The water temperature was 25 °C.

$U = 2$ m/s. Then it increases more rapidly and reaches the height of the viscous layer (1 mm) at 4 m/s. At higher wind speeds the rear face of the spectrum becomes saturated and the peak moves towards lower frequencies. The spectrum at 43 rad/s frequency thus shows the overshooting which is not visible in the characteristic wave height and therefore the values of these two parameters are no longer closely related.

As the wind speed is increased from zero in small increments the appearance of the surface goes through several distinct stages. At very low wind speeds the disturbances in the surface can be discerned from the irregularity of reflected images. The slopes are so small that it is not possible to see by eye that the waves are progressive. However, the good agreement between the measured surface displacement spectrum and that calculated from slope measurements shows that the waves obey the theoretical dispersion relation (3) used to transform slope to displacement. At somewhat higher windspeeds ($U = 3.1$ m/s) the first distinctly wavelike disturbances can be detected by eye. Between these two wind speeds there is a continuous change in slope and elevation variances as detected by the various measuring methods. We define the higher wind speed, where the surface patterns are distinctly wave-like and progressive in the wind direction, as the critical wind speed. The r.m.s. slope which corresponds to this visual definition was 6.6 m radians, and this slope therefore defines the critical wind speed. The spectrum $S(\omega)$ at $\omega = 43$ rad/s was approximately 6.5×10^{-11} m^2 s/rad at this critical slope, and the characteristic wave height was about 0.3 mm.

Other laboratory experiments devised to determine the critical wind speed usually conclude that centreline speeds of about 3 m/s are required to generate visually perceptible waves. Field observations, on the other hand, suggest considerably lower
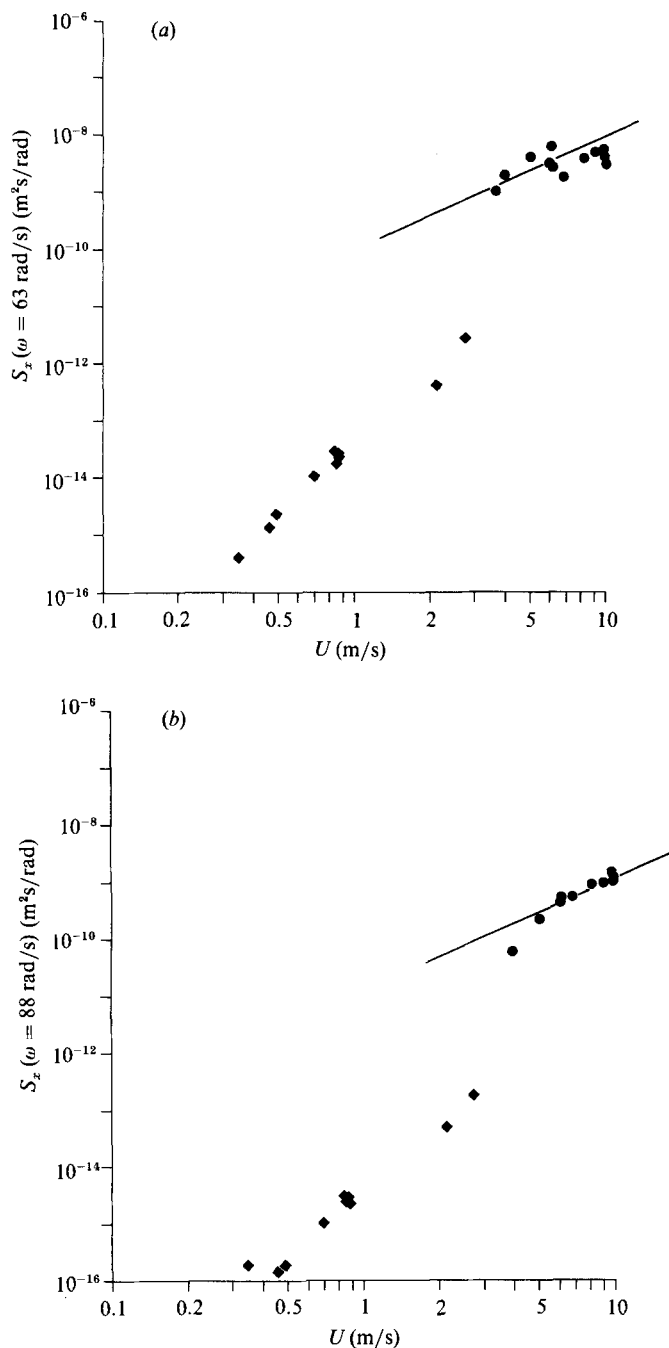
FIGURE 8. Growth with wind speed of single components on the rear face of the wave spectrum. ●, capacitance gauge; ◆, transformed from slope gauge. The line has a slope of 2.

values. The explanation seems to be that the critical wind speed is fetch dependent and the close agreement between different laboratory experiments merely reflects the narrow range of tank sizes used in these experiments.

Pierson & Stacy (1973) studied the wind dependence of high-frequency waves in a tank. They found that their parameter D, which describes the energy level of
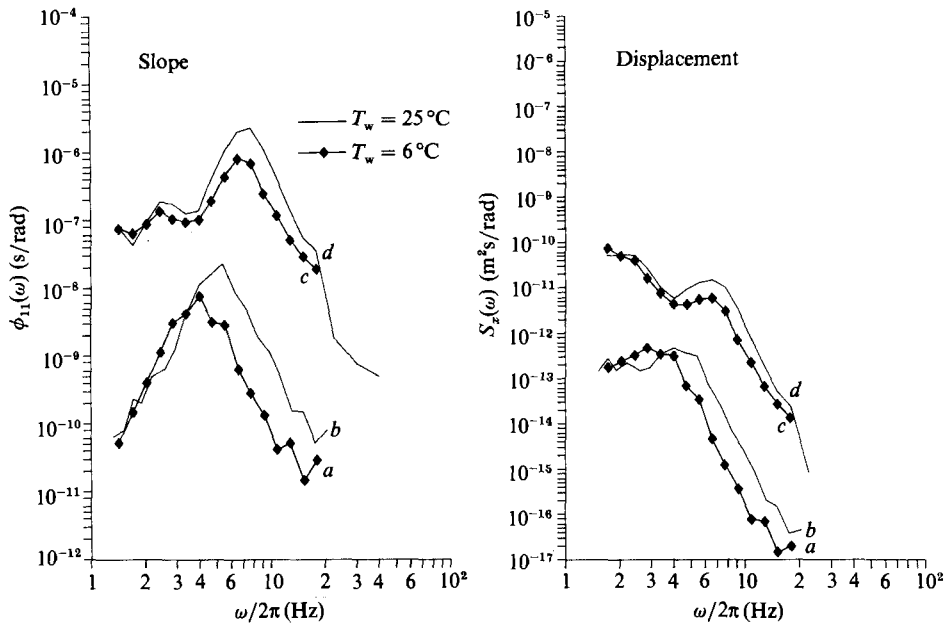
FIGURE 9. Displacement and slope spectra at two temperatures. (a) $T_w = 6$ °C, $U = 0.76$ m/s; (b) $T_w = 25$ °C, $U = 0.48$ m/s; (c) $T_w = 6$ °C, $U = 2.9$ m/s, $U_N = 2.7$ m/s; (d) $T_w = 25$ °C, $U = U_N = 2.8$ m/s.

the rear face of the spectrum (D is closely related to the more common Phillips saturation range parameter α), very sharply increases by three orders of magnitude at $u_* = 12$ cm/s. Their data, which covers a fetch range from 2.3 m to 6.4 m, did not indicate any fetch dependence, and Pierson & Stacy concluded that $u_* = 12$ cm/s, corresponding to $U_{19.5} = 3$ m/s, is the critical wind speed. On the other hand, Pokazeyev & Voronin (1982) found a clear fetch dependence of U_{cr}. They also used the sudden increase as a definition of their U_{cr} and reported 4.9–5.4 m/s at 1.2 m fetch and 3.4–3.7 m/s at 4.6 m fetch. We believe that these inconsistencies reflect the various sources of background noise, surface contamination and limited accuracy of the wave gauges used (cf. §2).

A similar, but not as large, jump can be seen in our data at 10 Hz and higher frequencies, i.e. above the peak (figure 8). The instability theory predicts a sharp rise of the spectrum directly from the background level; while our data show a gentle initial increase followed by a pronounced jump. However, the steepness of our jump and that predicted from the theory are comparable.

The jump seems to occur in our data at a slightly smaller friction velocity than predicted by Kawai, but neither our measurements of u_* nor the growth rates deduced from the figures in Kawai (1979b) are accurate enough to make very exact comparisons possible in this wind speed range.

3.3. *Temperature effect*

The viscosity of water ν_w changes considerably with temperature, from 1.8×10^{-6} m²/s at 0 °C to 0.8×10^{-6} m²/s at 30 °C (Weast 1970). The viscous decay rate $\beta_s = -4k^2\nu_w$ is important at the wavelength of the initial waves ($\lambda \approx 8$ cm) and therefore the critical wind speed should depend on temperature. If the growth mechanism of initial waves is exponential the inception wind speed should also depend on temperature.
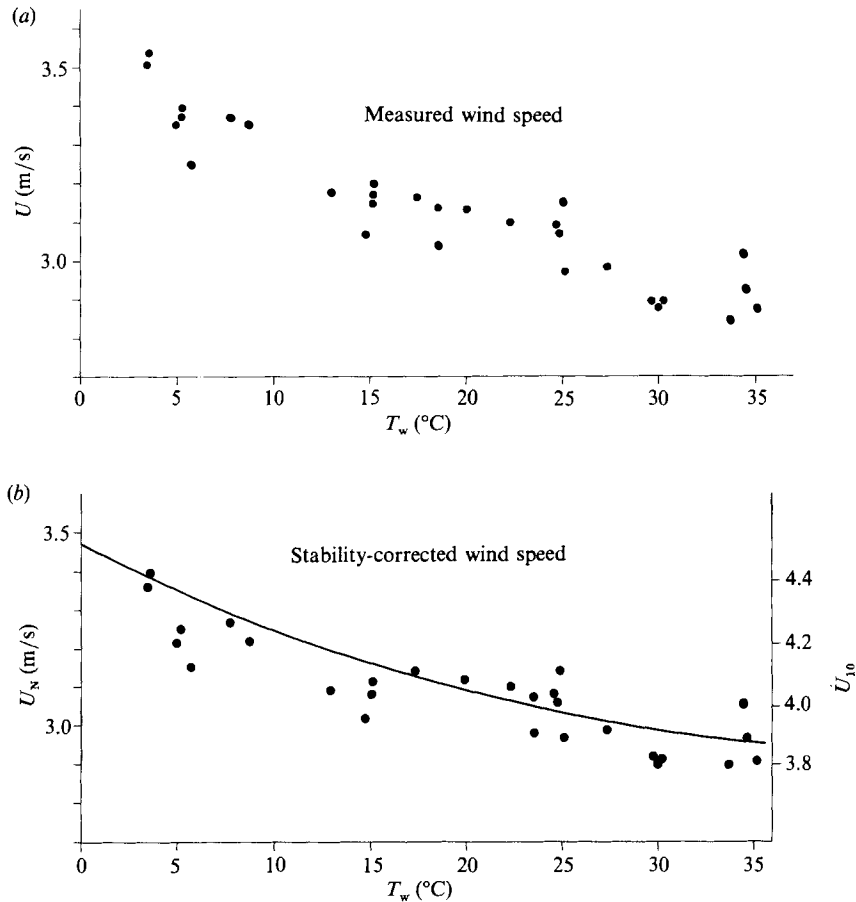
FIGURE 10. Critical wind speed at 0.156 m height *vs.* temperature. The 6.6 mrad r.m.s. slope at the critical wind speed was determined by the visual method. The line (figure 10b) shows the predicted temperature dependence based on our observed β at fixed 25 °C temperature (figure 6) and assuming $\beta_{\rm d} = -4\,k^2\nu_{\rm w}$.

Because $\beta_{\rm s}$ increases rapidly with k, the wavelength of the initial waves should be longer at lower temperatures.

The spectra measured at 6 °C (figure 9) show these effects clearly. Assuming that the growth is exponential the inception wind speed seems to be about 0.7 m/s and the wavelength of the initial waves was 10–15 cm. The corresponding values at 25 °C were $U \approx 0.4$ m/s ($u_* \approx 2$ cm/s) and wavelength 7–10 cm. At $\omega = 63$ rad/s (10 Hz) the spectrum at $U = 0.83$ m/s and $T_{\rm w} = 6$ °C was at about the same level as the spectrum at $U = 0.45$ m/s and $T_{\rm w} = 25$ °C; the spectral density at $U = 0.85$ m/s and $T_{\rm w} = 25$ °C was 30 times larger.

In the shear-flow instability theory the friction velocity u_* is the controlling variable for the growth of the initial wavelets. Since we were unable to control the air temperature, changes in water temperature produce changes in stability of the air boundary layer. Therefore, either u_* should be used for the comparison or U should be corrected for stability to reveal the viscosity effect on the inception wind speed. Although U itself could be measured rather accurately, the stability correction to recover the equivalent neutral U (inception) became so large that the results were not
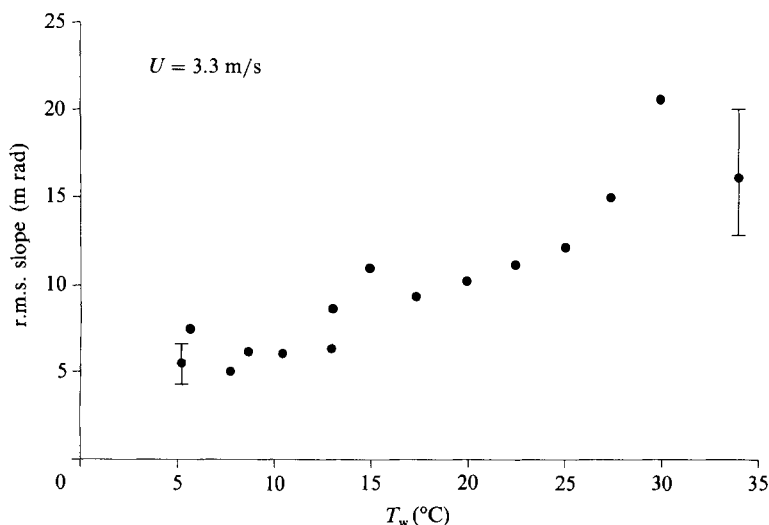
FIGURE 11. Root-mean-square slope at fixed ($U = 3.3$ m/s) wind speed *vs.* water temperature. The bars refer to the $\pm 20\%$ accuracy of the visual measurement (cf. figure 2).

reliable. However, the change of the inception u_* (measured) with temperature was generally consistent with the prediction from viscous dissipation but the measured u_* at these very low wind speeds was too inaccurate to justify a more quantitative comparison.

At higher wind speeds (near the critical wind speed) the effects of stability are less pronounced and hence the stability correction less uncertain. At the critical wind speed (in which the r.m.s. slope is 6.6 mrad) the large amount of data obtained by the simplified visual method allows us to deduce the viscosity and temperature effect clearly. Figure 10 shows that the critical wind speed increases from $U = 2.9$ m/s at 35 °C to 3.5 m/s at 4 °C. The critical wind speed depends on fetch and these results apply only for the 4.7 m fetch. The wind speed is sufficiently high that only a small stability effect is included in the temperature effect. In figure 10 (*b*) the stability effect is removed and the wind speed shown is the equivalent neutral wind speed at the measurement height of 15.6 cm. The dependence of the critical wind speed on water temperature is evident –about a 10% change over 30 °C. The line is the expected temperature dependence deduced from the observed growth rate (β) at 25 °C and the theoretical temperature dependent viscous dissipation rate $\beta_s = -4\,k^2\nu_w$. We have assumed that the input rate β_i is relatively insensitive to changes in ν_w.

A similar calculation can be made using the growth rates given by Kawai's (1979*b*) theory. This yields a change of about 7% in u_* compared with the observed 10%.

Figure 11 shows how the r.m.s. slope increases at a fixed (3.3 m/s) wind speed at 4.7 m fetch. The increase from 5 mrad to 15 mrad roughly corresponds to 9 times increase in the spectral density, in reasonable agreement with the calculated increase of 8 times that is obtained using our observed growth rates.

4. Discussion

4.1. Fetch dependence of the critical wind speed

In this experiment we have made measurements at a single fetch and, indeed, other laboratory experiments with similar goals have been performed over a rather restricted range of fetches (1 m to 10 m). However, if we are to infer the critical wind speed observable on lakes and oceans, fetch dependence is at the heart of the matter. As remarked before, the inception wind speed is expected to be insensitive to fetch. The critical speed, on the other hand, will be very fetch dependent since it is the speed at which the surface disturbances are readily observable by the naked eye. Once the exponential growth rate β becomes positive, growth will continue down-fetch until eventually the waves are limited by saturation, so that the larger the fetch the lower the critical wind speed, until in the limit of very large fetch it approaches the wind speed at which β becomes positive.

If the variability of the wind is small so that β can be approximated as a linear function of U, one should be able to discern surface disturbances on open water bodies (with sufficient fetch) when the average wind speed exceeds the wind speed when β becomes positive. However, at such low wind speeds natural winds are usually gusty and patchy, as the appearance of transitory 'cats-paws' illustrates, and the standard deviation of the wind speed may be 50 % of the wind speed itself. The waves may decay below the readily observable limit between gusts, although β for the average wind speed is positive. In addition, the viscous damping is extremely sensitive to surface contamination and therefore the wave field will be patchy until the contamination has drifted away or mixed into the bulk of the water. Thus, if we require that the surface be totally covered by readily observable waves at the critical wind speed we should expect that this critical wind speed be somewhat higher than the wind speed when β becomes positive. As much as anything, the scatter of the observed critical wind speeds at long fetches (e.g. Scott Russell 1844, 0.85 m/s; Jeffreys 1924, 1.1 m/s; Roll 1951, 0.4 m/s; Van Dorn 1953, 2 m/s) reflects the observer's choice of when the surface is adequately covered with wavelets. Both Jeffreys and Van Dorn report disturbances on the surface below the wind speed they consider critical.

Even with an objective choice of surface roughness and its uniformity corresponding to the critical wind speed, the latter still remains dependent on surface temperature, surface contamination and wind stability and gustiness that may depend on the recent history of the passage of air over the terrain surrounding the water body. The difficulties of obtaining an estimate of U_{cr} from natural water bodies are further exacerbated by the conflicting requirements of longer fetch and no background wave energy. Perhaps all that can be said is that the observed U_{cr} values (0.4 to 2 m/s) are in general agreement with the inception wind speed deduced from our laboratory experiments. In order to explore the matter further, measurements of wind gustiness, boundary-layer stability, water temperature and surface contamination are required in addition to wave spectra.

4.2. The Phillips mechanism

The conclusion from 3.1 is that the observed growth rates are not consistent with the predictions from the linear, viscous, coupled shear-flow instability mechanism. This could mean that the theory simply underpredicts the exponential growth at very low wind speeds. It could also mean that the instability mechanism (which is

characterized by exponential growth) is not the only important contributor to the growth of initial waves. (We want to point out here that although the input from vibrations in (5) is linear with time or fetch it is not an alternative explanation for the observed growth unless it is strongly wind dependent.)

Previous laboratory experiments at higher wind speeds have not revealed the linear growth phase predicted by the Phillips resonance mechanism (Phillips 1957). At very low wind speeds when both the exponential growth rate and the wave height are small the contribution from the resonance mechanism might be relatively more important. In the following we explore the possibility that the observed growth at the peak of the spectrum can be explained by the Phillips resonance mechanism acting alone.

In the initial stage, when the exponential growth is insignificant, the growth by the resonance mechanism, in absence of any dissipative processes, is given by (Phillips 1957)

$$F(\boldsymbol{k}, t) = \frac{\pi}{\rho_w^2 c^2} \Pi(\boldsymbol{k}, \omega) t, \tag{11}$$

where $F(\boldsymbol{k}, t)$ is the wavenumber spectrum, $\Pi(\boldsymbol{k}, \omega)$ is the spectrum of turbulent pressure fluctuations in the air flow and t is time.

The three-dimensional pressure spectrum $\Pi(\boldsymbol{k}, \omega)$ is not well known and, in particular, the extrapolation to wind speeds below 1 m/s is uncertain. We therefore try to calculate only a first approximation using simplifying assumptions that allow us to use the frequency spectrum of the pressure fluctuations. The first assumption is that the turbulence is frozen:

$$\Pi(\boldsymbol{k}, \omega) = \Pi(\boldsymbol{k}) \, \delta(\omega - \boldsymbol{k} \cdot U_c),$$

where δ is the Dirac delta function. Here U_c is the convection velocity, which according to Elliott (1972) is approximately the wind speed at height π/k. We then consider only waves whose phase speed equals the wind speed. Under the frozen turbulence assumption the resonance condition for these waves is fulfilled only if they travel in the direction of the wind. In reality the fluctuations are not rigidly convected with the mean wind speed, but lose their coherence as they propagate. We will not write an explicit functional form for the resulting softening of the delta function, but simply integrate (11) over a band which corresponds to the width of the observed peak in figure 4. This gives us the average spectral density of the peak in the frequency band $\Delta\omega$

$$S(\omega, t) = \frac{2\pi U_c^2}{\Delta\omega \, \rho_w^2 c^2} \Pi_\omega(\omega) t. \tag{12}$$

This equation can be used only if the phase speed of the waves equals the wind speed U_c. The accurate wind speeds for the spectra labelled by the 0.5 m/s label in figure 4 are 0.48 m/s and 0.46 m/s. This corresponds to about 0.35 m/s at 3.5 cm height. Waves that have this phase speed have 7 cm wavelength and their frequency is 30 rad/s (4.8 Hz). The peaks in figure 4 are at 26 rad/s and 32 rad/s. It is worth noting that at these low wind speeds the phase speed $c(k)$ and the convection wind speed at height π/k are closely matched over a wide range of k, so that the resonance mechanism would be expected to produce growth over a wide wavenumber range as in figure 4.

Since the available pressure spectra were measured at higher wind speeds and at lower frequencies, we have to extrapolate them to $U = 0.47$ m/s and $\omega = 30$ rad/s.
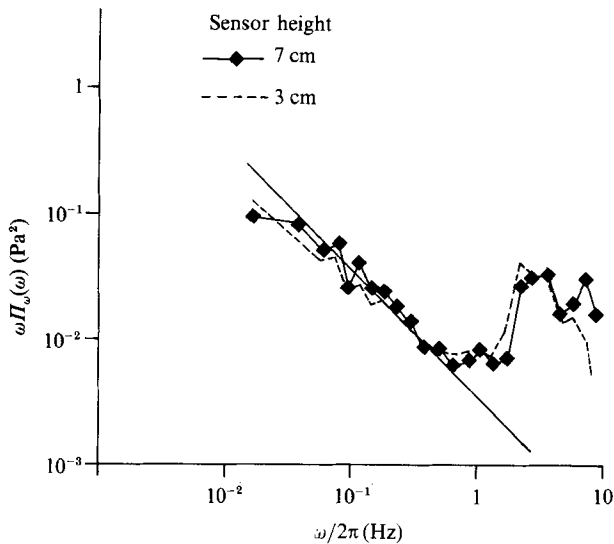
FIGURE 12. Frequency spectra of pressure fluctuations over water in a large wind wave flume ($x = 55$ m, water depth 1.2 m, height of the air flow 1.86 m) at $u_* = 18$ cm/s. The line shows the extrapolation into high frequencies where the measured spectra show wave-induced fluctuations and noise.

In wind tunnels pressure data above solid surfaces have been successfully scaled by

$$\omega\Pi(\omega)/\rho_a^2 u_*^4 = \Phi(\omega\gamma/U),$$

where γ is the boundary-layer thickness and Φ a dimensionless function.

We first use the pressure fluctuation measurements that were made over water in the large wind-wave flume at our laboratory using a disk sensor for the static pressure of the type described by Elliott (1972). Figure 12 shows the spectra and the ω^{-2} power law which was used in the scaling. Equation (12) gives at 4.7 m fetch $S(\omega) = 1.3 \times 10^{-12}$ m^2 s/rad, which is slightly higher than the observed spectrum 6×10^{-13} m^2 s/rad in figure 4.

Equation (12) ignores the dissipation by viscosity. This dissipation depends on amplitude whereas the input from the resonance mechanism is independent of the amplitude. As the waves grow the spectrum reaches the height where the dissipation balances the input. In the conditions above, this will occur when $S(\omega) = 1.0 \times 10^{-12}$ m^2 s/rad.

For comparison we used the data from Elliott (1972) who measured atmospheric pressure fluctuations over water. Elliott could not determine the height of the boundary layer which leaves the scaling open. Assuming it to be the same in both cases the spectrum at $x = 4.7$ m is $S(\omega) = 1.1 \times 10^{-12}$ m^2 s/rad if dissipation is ignored, and the asymptotic value with dissipation is 9×10^{-13} m^2 s/rad. In the field we therefore can expect the Phillips mechanism to generate the same size waves that we observed in our flume at the inception wind speed and fetch of 4.7 m. Since in our flume the height of the boundary layer must be much smaller than in the atmospheric boundary layer, the scaling by the boundary-layer height suggests even higher growth in the laboratory, however, this scaling between laboratory and field has not been verified.

It therefore seems possible that Phillips resonance mechanism is effective enough

to generate the observed spectrum at very low wind speeds. At higher winds the situation becomes complicated. The waves in our flume cannot travel at the wind speed of $U = 2$ m/s and above. Estimates of the growth would require knowing the full three-dimensional pressure spectrum. However, it seems unlikely that the resonance mechanism at higher wind speeds could contribute significantly to our observed spectra.

There is one additional fact that points towards the Phillips resonance mechanism as an initiation mechanism: mechanical waves show small exponential growth rates at low wind speeds (Wilson *et al.* 1973; Gottifredi & Jameson 1970) that agree with the shear-flow instability theory better than our experiment or the data of Larson & Wright (1975). This is understandable if we assume that the mechanical waves were already high enough for the exponential growth to dominate.

If the Phillips mechanism is indeed the initiation mechanism the inception wind speed depends on the appearance of turbulent fluctuations that have the right wavenumbers and that are convected at least at the minimum phase speed of surface waves, 23 cm/s. It is interesting that the wind speed at height π/k falls below the phase speed of waves $c(k)$ for all wavenumbers when the wind at the centre of our flume is 0.4 m/s and less. This is the wind speed when the measured spectrum is estimated to rise above the calculated background S_{xp} (at the floating plate at zero fetch). Ursell (1956) has pointed out that even turbulent fluctuations with zero mean motion could generate some undulations on the surface. However, without resonance the efficacy of such a mechanism would be very low, and we would not expect to detect any additional wave energy above the background until the wind speed exceeds the minimum phase speed.

5. Conclusions

Questions related to the minimum wind speed needed to excite surface waves are difficult to explore in the field because of the pronounced effects of variables that are essentially uncontrollable, such as wind gustiness and surface cleanness. In the laboratory, on the other hand, the waves are very small and masked by other oscillations that are generated by microseisms. In the laboratory experiment reported here we were able to measure the growth of very small waves starting from a very weak background induced by microseisms. The growth rates measured at very low wind speeds were significantly larger than those predicted by all recent treatments of the coupled shear-flow instability theory (Valenzuela 1976; Kawai 1979; van Gastel *et al.* 1985). On the assumption that our observed wave growth is due to an instability mechanism (exponential growth), we find that the friction velocity at which the growth rate β becomes positive ($u_* \approx 2$ cm/s) is less than half that predicted by the instability theory ($u_* \approx 4$–5 cm/s). The wavelength of the fastest growing waves, once β is positive, was observed to be 7–10 cm at water temperature of 25 °C. This agrees well with Kawai's (1979) calculations, but the recent and more refined theory of van Gastel *et al.* (1985) yields only 2 cm. The observed initial wavelength was dependent on water temperatures, being approximately 10–15 cm at water temperature of 5 °C. The increased viscosity at lower temperatures reduces the growth rate of the shorter waves and forces the initial waves to longer wavelengths.

Insofar as this experiment is a test of the instability theory, the theory appears unable to explain the key observation of the friction velocity for initiating growth of wind waves. However, an alternate hypothesis is that the initial growth of water

waves under a turbulent wind is dominated by some mechanism other than that described by the shear-flow instability theory. In this context, we have estimated the efficacy of Phillips (1957) resonance mechanism from observations of the turbulent pressure spectrum in light winds in a laboratory wind-wave tank and found that it is capable of accounting for the observed initial growths. However, we cannot be certain that the resonance mechanism, rather than shear-flow instability, dominates the process of wave growth in very light winds, because the calculations of growth via resonance with intrinsic pressure perturbations depend on assumptions of the approximate integral timescale of the pressure fluctuations and of the correct scaling lengths for the pressure spectrum. Perhaps a detailed experimental investigation of the ingredients for an accurate calculation of Phillips' mechanism is overdue, but it is, regrettably, outside the scope of this work. Nonetheless we may conclude that either the growth of waves in very light winds is accomplished by some agency other than shear-flow instability or that the shear-flow instability calculations do not agree with the observations when waves first form.

If the waves are indeed initiated by shear-flow instability then our observations suggest the inception wind speed (first positive growth) is about 0.7 m/s referred to 10 m height. On the other hand, Phillips' resonance mechanism requires that the wind speed exceeds the minimum phase speed of the slowest waves ($c = 0.23$ m/s, $\lambda = 0.17$ m). Since pressure perturbations of scale λ are convected at the wind speed at height $\frac{1}{2}\lambda$ (Elliott 1972), this corresponds to a 10 m wind speed of about 0.7 m/s also. This estimate from either cause does not conflict seriously with observations at long fetch of the minimum wind speed for wave growth. The lowest well-documented field observations of the minimum wind speed appear to be those of Roll (1951), who reports 0.4 m/s measured at 35 cm height, which corresponds to a 10 m wind speed of about 0.6 m/s.

When the waves grow to be sufficiently large that they are readily observable visually, their observed growth rates are in fairly good agreement with the shear-flow instability calculations. For these visually observable waves we estimated their dependence on surface temperature. This temperature dependence could be predicted by using the growth rate curves we observed at 25 °C and applying the theoretical temperature-dependent viscous damping.

It appears likely that waves are first formed at very light winds by an amplitude-independent Phillips-type resonance mechanism and they grow until balanced by amplitude dependent viscous damping or if the wind increases slightly the shear flow instability (also amplitude dependent) mechanism may overcome the viscous damping and quickly dominate the growth phase.

REFERENCES

ATAKTÜRK, S. S. & KATSAROS, K. B. 1987 Intrinsic frequency spectra of short gravity–capillary waves obtained from temporal measurements of wave height on a lake. *J. Geophys. Res.* **92**, C5, 5131–5141.

BENJAMIN, T. B. 1959 Shearing flow over a wavy boundary. *J. Fluid Mech.* **6**, 161–205.

BRUNE, J. N. & OLIVER, J. 1959 The seismic noise of the earth's surface. *Bull. Seismol. Soc. Am.* **49**, 439–453.

ELLIOTT, J. A. 1972 Microscale pressure fluctuations measured within the lower atmosphere boundary layer. *J. Fluid Mech.* **53**, 351–383.

GASTEL, K. VAN, JANSSEN, P. A. E. M. & KOMEN, G. J. 1985 On phase velocity and growth rate of wind-induced gravity–capillary waves. *J. Fluid Mech.* **161**, 199–216.

GOTTIFREDI, J. C. & JAMESON, G. J. 1970 The growth of short wave on liquid surfaces under the action of a wind. *Proc. R. Soc. Lond.* A **319**, 373–397.

HUGHES, B. A. & GRANT, H. L. 1974 The interaction of wind waves and internal waves: experimental measurements. *Defence Research Establishment Pacific, Victoria, BC. Rep.* 74-1.

HUNT, J. N. 1952 Viscous damping of waves over an inclined bed in a channel of finite width. *Houille Blanche* **7**, 836–842.

JEFFREYS, H. 1924 On the formation of water waves by wind. *Proc. R. Soc. Lond.* A **107**, 189–206.

KAWAI, S. 1979*a* Generation of initial wavelets by instability of a coupled shear flow and their evolution to wind waves. *J. Fluid Mech.* **93**, 661–703.

KAWAI, S. 1979*b* Discussion on the critical wind speed for wind wave generation on the basis of shear-flow instability theory *J. Ocean Soc. Japan* **35**, 179–186.

KEULEGAN, G. H. 1951 Wind tides in small closed channels. *J. Res. Natl Bur. Stand.* **46**, 358–381.

KUNISHI, H. 1957 Studies on wind waves with use of wind flume (I). On the shearing flow in the surface boundary layer caused by wind stress. *Ann. Disas. Prev. Res. Inst., Kyoto Univ.* **1**, 199–127.

LAMB, H. 1932 *Hydrodynamics*. Cambridge University Press.

LARSON, T. R. & WRIGHT, J. W. 1975 Wind-generated gravity–capillary waves: laboratory measurements of temporal growth rates using microwave backscatter. *J. Fluid Mech.* **70**, 417–436.

LONGUET-HIGGINS, M. S. 1950 A theory of microseisms. *Phil. Trans. R. Soc. Lond.* A **243**, 1–35.

MILES, J. W. 1962 On the generation of surface waves by shear flows. Part 4. *J. Fluid Mech.* **13**, 433–448.

PHILLIPS, O. M. 1957 On the generation of waves by turbulent wind. *J. Fluid Mech.* **2**, 417–495.

PIERSON, W. J. & STACY, R. A. 1973 The elevation, slope and curvature spectra of a wind roughened sea surface. *NASA Contractor Rep.* CR-2646.

PLATE, E. J., CHANG, P. C. & HIDY, G. M. 1969 Experiments on the generation of small water waves by wind. *J. Fluid Mech.* **35**, 625–656.

POKAZEYEV, K. V. & VORONIN, L. M. 1982 Initial stage of wind-wave development. *Izv. Atmos. Ocean. Phys.* **18**, 689–691.

ROLL, H. U. 1951 Neue Messungen zur Entstehung von Wasserwellen durch Wind. *Ann. Met., Hamburg* **4**, 269–286.

SCHLICHTING, H. 1968 *Boundary-Layer Theory*, 6th edn. McGraw-Hill.

SCOTT RUSSELL, J. 1844 Report on waves. *Rep. Brit. Assn* 317–318.

STALDER, J. J. 1957 The development of a capacity probe for measuring capillary waves. *Tech. rep. prepared for the Electronics Branch of the Office of Naval Research under contract* N ONR 285(26).

TENNEKES, H. & LUMLEY, J. L. 1972 *A First Course in Turbulence*. MIT Press.

URSELL, F. 1956 *Wave Generation by Wind, in Surveys in Mechanics*, pp. 216–249. Cambridge University Press.

VALENZUELA, G. R. 1976 The growth of gravity–capillary waves in a coupled shear flow. *J. Fluid Mech.* **76**, 229–250.

VAN DORN, W. G. 1953 Wind stress on an artificial pond. *J. Mar. Res.* **12**, 249–276.

WEAST, R. C. 1970 *Handbook of Chemistry and Physics*, 50th edn. The Chemical Rubber Company.

WILSON, W. S., BANNER, M. L., FLOWER, R. J., MICHAEL, J. A. & WILSON, D. G. 1973 Wind-induced growth of mechanically generated water waves. *J. Fluid Mech.* **58**, 435–460.

WRIGHT, J. W. 1966 Backscattering from capillary waves with application to sea clutter. *IEEE Trans. on Aut. and Prop.* Ap-14, 749–754.

WU, J. 1978 A note on minimum wind stress for wave inception. *Tellus* **30**, 93–96.